KURENAI 紅

Kyoto University Research Information Repository

KYOTO UNIVERSITY

Title	Temporal variations in magnetic signals generated by the piezomagnetic effect for dislocation sources in a uniform medium
Author(s)	Yamazaki, Ken'ichi
Citation	Geophysical Journal International (2016), 206(1): 130-141
Issue Date	2016-07
URL	http://hdl.handle.net/2433/252358
Right	This article has been accepted for publication in Geophysical Journal International ©: 2016 The Author Published by Oxford University Press on behalf of the Royal Astronomical Society. All rights reserved.
Type	Journal Article
Textversion	publisher

Temporal variations in magnetic signals generated by the piezomagnetic effect for dislocation sources in a uniform medium

Ken'ichi Yamazaki

Miyazaki Observatory, Disaster Prevention Research Institute, Kyoto University, 3884 *Kaeda, Miyazaki* 889–2161, *Japan.*
E-mail: *kenichi@rcep.dpri.kyoto-u.ac.jp*

SUMMARY

Fault ruptures in the Earth's crust generate both elastic and electromagnetic (EM) waves. If the corresponding EM signals can be observed, then earthquakes could be detected before the first seismic waves arrive. In this study, I consider the piezomagnetic effect as a mechanism that converts elastic waves to EM energy, and I derive analytical formulas for the conversion process. The situation considered in this study is a whole-space model, in which elastic and EM properties are uniform and isotropic. In this situation, the governing equations of the elastic and EM fields, combined with the piezomagnetic constitutive law, can be solved analytically in the time domain by ignoring the displacement current term. Using the derived formulas, numerical examples are investigated, and the corresponding characteristics of the expected magnetic signals are resolved. I show that temporal variations in the magnetic field depend strongly on the electrical conductivity of the medium, meaning that precise detection of signals generated by the piezomagnetic effect is generally difficult. Expected amplitudes of piezomagnetic signals are estimated to be no larger than 0.3 nT for earthquakes with a moment magnitude of ≥ 7.0 at a source distance of 25 km; however, this conclusion may not extend to the detection of real earthquakes, because piezomagnetic stress sensitivity is currently poorly constrained.

Key words: Electromagnetic theory; Magnetic and electrical properties; Wave propagation; Early warning.

1 INTRODUCTION

Fault ruptures in the Earth's crust generate both elastic and electromagnetic (EM) signals. Following the ruptures, ground motions (i.e. seismic waves) propagate through the solid Earth and deform the crust. This generates EM waves through a variety of mechanisms, including the motional induction effect (e.g. Gershenzon *et al.* 1993; Gao *et al.* 2014), the electric kinetic effect (e.g. Ishido & Mizutani 1981; Pride 1994), the piezomagnetic effect (Yamazaki 2011a,b), the piezoelectric effect (e.g. Bishop 1981; Huang 2002), and the resonance of ions (Honkura *et al.* 2009; Kuriki *et al.* 2011; Matsushima *et al.* 2013). Because the maximum speed of EM wave propagation is c (3.0×10^8 m s^{-1}), much faster than elastic waves ($\sim 10^4$ m s^{-1}), EM signals generated by any of these mechanisms should appear before seismic wave arrivals at any point where they can be detected.

A key aspect of earthquake-related EM phenomena is just how large the EM signals are likely to be. In particular, would the EM signals that precede the arrival of seismic waves be of sufficient amplitude for detection. If the answer is yes, then it would be possible to use EM observations to provide early warnings of earthquakes. At present, early earthquake warning is completely reliant on seismic observations. A number of authors have reported EM signals coetaneous with earthquake ground motion (e.g. Eleman 1965; Nagao *et al.* 2000; Skordas *et al.* 2000; Abdul Azeez *et al.* 2009; Honkura *et al.* 2009); however, some of these signals may be due to physical motion of the EM sensor. In contrast, few reports have been published on EM phenomena that precede seismic wave arrivals, except for a recent report for the M_w 6.9 Iwaki-Miyagi, Japan earthquake (Okubo *et al.* 2011). However, because geomagnetic observations are sparse compared with seismic and geodetic observations, it is possible that such phenomena have not been reported simply because of insufficient opportunities for observation. Therefore, theoretical approaches are required, along with efforts to refine observations.

Theoretical approaches involve calculations of the expected amplitudes of EM signals generated from elastic waves by a variety of conversion mechanisms. Earlier works have established a theoretical framework for mechanisms such as the electrokinetic effect (e.g. Pride & Haartsen 1996; Haartsen & Pride 1997; Garambois & Dietrich 2001, 2002; Ren *et al.* 2012; Gao *et al.* 2013a,b), motional induction (e.g. Gershenzon *et al.* 1993, 2014; Gershenzon & Bambakidis 2001; Yamazaki 2012; Gao *et al.* 2014), and the piezoelectric effect (e.g. Russell

& Barker 1991; Ogawa & Utada 2000a,b). However, these studies have not covered the entire possible range of EM sources in the Earth's crust; thus, studies of unconsidered mechanisms are still required to fully characterize elastic-EM conversions due to seismic waves.

This study focuses on the piezomagnetic effect as a mechanism of generating EM phenomena through the conversion of elastic waves. The piezomagnetic effect describes changes in magnetization of ferromagnetic minerals under the application of mechanical stresses (e.g. Stacey 1964; Nagata 1970a,b; Stacey & Johnston 1972; Zlotnicki *et al.* 1981). Many previous studies of geophysical phenomena related to the piezomagnetic effect are considered in a framework of elasto-statics, meaning that only the offsets in values before and after the stress changes are considered. The procedures and useful formulae for calculations in this framework have already been derived (e.g. Sasai 1991; Utsugi *et al.* 2000). This effect has been used to explain offsets in the geomagnetic field before and after earthquakes (e.g. Stuart *et al.* 1995; Sasai & Ishikawa 1997), and during magma intrusion at active volcanoes (e.g. Ueda *et al.* 2006; Napoli *et al.* 2008). In contrast, few studies have investigated the time-dependent EM field caused by the piezomagnetic effect. An earlier work by Utsugi (2010) has dealt with this topic, but it ignores the effects of finite conductivity of Earth's crust. Recent works by Yamazaki (2011a,b) have also dealt with the time-dependent EM field caused by the piezomagnetic effect, but they only considered far-field seismic waves. Evaluating the amplitudes of EM signals generated by the piezomagnetic field, including near-field contributions and the effects of finite conductivity, is an important challenge in investigations of earthquake-related EM signals.

The remainder of this paper is organized as follows. In Section 2, the problem is framed and the governing equations are derived. In Section 3, I derive a set of analytical solutions in the time domain. In Section 4, numerical examples are used to analyse the behaviour of the solution. In Section 5, the implications of the results are discussed. Finally, the conclusions are presented in Section 6.

2 DEFINITIONS OF THE PROBLEM AND GOVERNING EQUATIONS

The situation is considered in which external forces are applied to a point in an elastic whole-space medium with a uniform magnetization. The following phenomena are expected. First, elastic deformation and stress changes propagate within the medium. Next, changes in magnetization are associated with elastic deformation by the piezomagnetic effect. Finally, variations in the EM field are excited by changes in magnetization. Therefore, the expected phenomena can be described by the momentum equation, the stress–strain relationship for elastic media, the constitutive law for the piezomagnetic effect, and Maxwell's equations for EM fields. Below, each equation is given, together with additional assumptions required for analytical solution.

2.1 Displacement and stress in a homogeneous elastic medium

It is assumed that the displacement vector field $\mathbf{u} = (u_i)$ and stress tensor field $\boldsymbol{\tau} = (\tau_{ij})$ are related by Hooke's law:

$$\tau_{ij} = \lambda \delta_{ij} \frac{\partial u_k}{\partial x_k} + \mu \left(\frac{\partial u_i}{\partial x_j} + \frac{\partial u_j}{\partial x_i} \right), \tag{1}$$

where λ and μ are scalar elastic constants and δ_{ij} is the Kronecker delta. Herein, the Einstein summation convention for subscripts are applied. The displacement field $\mathbf{u}$ obeys the momentum equation:

$$\rho \frac{\partial^2}{\partial t^2} \mathbf{u}(\mathbf{x}, t) = \mathbf{F}(\mathbf{x}, t) + (\lambda + 2\mu)\nabla[\nabla \cdot \mathbf{u}(\mathbf{x}, t)] - \mu \nabla \times \nabla \times \mathbf{u}(\mathbf{x}, t), \tag{2}$$

where ρ is mass density, $\mathbf{x}$ is position, t is time and $\mathbf{F}$ is external forces applied to the medium (e.g. Aki & Richards 2002). Because a uniform medium is considered, λ, μ and ρ do not depend on location $\mathbf{x}$. In this situation, solution of eq. (2) for a single force at a point can be expressed analytically as described in the next section, and the stress field $\boldsymbol{\tau}$ is determined in terms of eq. (1).

2.2 Changes in magnetization via the piezomagnetic effect

A change in stress induces a change in magnetization via the piezomagnetic effect. Experimental results and theoretical considerations of the piezomagnetic effect (e.g. Stacey 1964; Nagata 1970a,b; Stacey & Johnston 1972; Zlotnicki *et al.* 1981) can be summarized by a simple linear relationship between changes in magnetization vector $\Delta\mathbf{J} = (\Delta J_i)$ and deviatoric stress tensor $\mathbf{T} = (T_{ij})$ (Sasai 1991):

$$\Delta J_i = \frac{3}{2}\beta T_{ij} J_j, \tag{3}$$

where β is a proportionality coefficient referred to as 'stress sensitivity', and $\mathbf{J} = (J_i)$ is the initial magnetization vector of the medium without applied stress. Now we consider a uniform medium; that is where $\mathbf{J}$ does not depend on location. For a uniform medium, the deviatoric stress tensor is given by

$$T_{ij} = \tau_{ij} - \frac{1}{3}\delta_{ij}\tau_{kk}. \tag{4}$$

The relationship (3) holds with sufficient accuracy when the magnitudes of applied stresses are within the range of those in the Earth's crust (e.g. Sasai 1991); thus, this is treated as the correct governing equation.

2.3 EM fields generated by time-varying magnetization

Temporal and spatial variations in the EM field are described by Maxwell's equations. In this study, the time-varying magnetization density $\Delta \mathbf{J}$ is the source of EM variations. Maxwell's equations involving $\Delta \mathbf{J}$ can be expressed in differential form as

$$\nabla \cdot \mathbf{E}(\mathbf{x}, t) = \frac{1}{\varepsilon} \rho_e(\mathbf{x}, t) \tag{5}$$

$$\nabla \cdot \mathbf{B}(\mathbf{x}, t) = 0 \tag{6}$$

$$\nabla \times \mathbf{E}(\mathbf{x}, t) + \frac{\partial}{\partial t} \mathbf{B}(\mathbf{x}, t) = \mathbf{0} \tag{7}$$

$$\nabla \times \{\mathbf{B}(\mathbf{x}, t) - \mu_{\mathrm{m}} \Delta \mathbf{J}(\mathbf{x}, t)\} = \mu_{\mathrm{m}} \mathbf{I}(\mathbf{x}, t) + \varepsilon \mu_{\mathrm{m}} \frac{\partial}{\partial t} \mathbf{E}(\mathbf{x}, t), \tag{8}$$

where $\mathbf{E}$ is the electric field, $\mathbf{B}$ is the magnetic field, $\mathbf{I}$ is electric current density, ρ_e is charge density, ϵ is electric permeability and μ_{m} is magnetic permeability. Variables x and t denote location and time, respectively. The magnetic permeability is usually denoted by μ with no subscript; however, in this manuscript the symbol μ has already been used for an elastic constant. For the same reason, charge density is denoted by ρ_e, to distinguish it from density.

Some simplification of the problem is required to derive analytical solutions. First, an isotropic form of Ohm's law for electric current density $\mathbf{I}$ is assumed, described by

$$\mathbf{I}(\mathbf{x}, t) = \sigma \mathbf{E}(\mathbf{x}, t), \tag{9}$$

where σ is scalar electrical conductivity. Because a whole-space medium is considered, σ is a constant. Second, it is assumed that the displacement current term (i.e. the second term in the right-hand side of eq. 8) is negligible. This assumption is reasonable because the dominant frequency of seismic waves is up to hundreds of Hz and the displacement current term is negligible compared with other terms, unless the frequency is extremely large (i.e. $\geq 10^4$ Hz). In fact, this is commonly assumed for EM phenomena in the solid Earth (e.g. Nabighian 1988, p. 8). Third, I assume μ_{m} does not depend on $\mathbf{B}$ and is equal to the magnetic permeability of a vacuum ($\mu_0 = 4\pi \times 10^{-7}$ H m^{-1}). This assumption is reasonable in the present problem, in which $\mathbf{B}$ fields generated by seismic waves are too small to affect μ_{m}.

Under the above assumptions, the governing equation of the magnetic field $\mathbf{B}$ is summarized by a single EM diffusion equation:

$$\nabla^2 \mathbf{B}(\mathbf{x}, t) - \mu_0 \sigma \frac{\partial}{\partial t} \mathbf{B}(\mathbf{x}, t) = -\mu_0 \nabla \times \nabla \times \Delta \mathbf{J}(\mathbf{x}, t). \tag{10}$$

Thus, the problem is to derive $\Delta \mathbf{J}$ for a given $\mathbf{F}$ in terms of eqs (1)–(4), then to determine $\mathbf{B}$ from eq. (10). Once $\mathbf{B}$ is determined, then the electric field $\mathbf{E}$ follows from eqs (8) and (9); rearranging these and combining terms yields

$$\mathbf{E}(\mathbf{x}, t) = \frac{1}{\sigma} \nabla \times \left[\frac{1}{\mu_0} \mathbf{B}(\mathbf{x}, t) - \Delta \mathbf{J}(\mathbf{x}, t) \right]. \tag{11}$$

3 DERIVATION OF THE GENERATED MAGNETIC FIELD

In this section, a solution to eq. (10) is derived that describes variations in the magnetic field generated by external forces via the piezomagnetic effect in a whole-space medium.

3.1 Expression of the source term

We can easily derive an expression for the source term of the governing equation; that is the right-hand side of eq. (10). Combining Hooke's law (eq. 1) with the constitutive law for the piezomagnetic effect (eqs 3 and 4), the changes in magnetization $\Delta \mathbf{J}$ in terms of $\mathbf{u}$ are

$$\Delta \mathbf{J} = \beta \mu \left[-(\nabla \cdot \mathbf{u})\mathbf{J} + \frac{3}{2} \nabla (\mathbf{u} \cdot \mathbf{J}) + \frac{3}{2} (\mathbf{J} \cdot \nabla) \mathbf{u} \right]. \tag{12}$$

Because we assume that $\mathbf{J}$ is constant, taking the curl of eq. (10) twice gives the expression

$$\nabla \times (\nabla \times \Delta \mathbf{J}(\mathbf{x})) = \beta \mu \left[-\nabla \times \{\nabla \times (\nabla \cdot \mathbf{u}(\mathbf{x}))\}\mathbf{J} + \frac{3}{2} (\mathbf{J} \cdot \nabla)\{\nabla \times (\nabla \times \mathbf{u}(\mathbf{x}))\} \right]. \tag{13}$$

Note that the argument t is omitted because this equation holds in both the frequency and time domains.

3.2 Impulse responses of the magnetic field

First, an expression is derived for **B** generated by a single force at the point $\mathbf{x} = (0, 0, 0)$. The explicit form of **u** is known as Stokes' solution, which appears in most seismology textbooks (e.g. Aki & Richards 2002, p. 101). For the case that the force F_p is expressed as $\delta(t)f_p$, with Dirac Delta function $\delta(t)$, an explicit form of the solution is given by

$$u_n(\mathbf{x}, t) = \frac{1}{4\pi\rho}(3x_n x_p - \delta_{np}r^2)\frac{1}{r^5}t\left\{H\left(t - \frac{r}{v_P}\right) - H\left(t - \frac{r}{v_S}\right)\right\}f_p$$
$$+ \frac{1}{4\pi\rho}\frac{1}{v_P^2}x_n x_p \frac{1}{r^3}\delta\left(t - \frac{r}{v_P}\right)f_p$$
$$- \frac{1}{4\pi\rho}\frac{1}{v_S^2}(x_n x_p - \delta_{np}r^2)\frac{1}{r^3}\delta\left(t - \frac{r}{v_S}\right)f_p, \tag{14}$$

where $r = |\mathbf{x}|$, H is the Heaviside step function, and v_P and v_S represent seismic P- and S-wave velocities, respectively. Seismic velocities v_P and v_S can be expressed in terms of λ and μ in eq. (2) as

$$v_P^2 = \frac{1}{\rho}(\lambda + 2\mu), \quad v_S^2 = \frac{1}{\rho}\mu. \tag{15}$$

The divergence and curl of **u** are given by

$$\nabla \cdot \mathbf{u}(\mathbf{x}, t) = \frac{1}{4\pi\rho v_P^2}(\mathbf{F} \cdot \nabla)\left\{\frac{1}{r}\delta\left(t - \frac{r}{v_P}\right)\right\}, \tag{16}$$

$$\nabla \times \mathbf{u}(\mathbf{x}, t) = -\frac{1}{4\pi\rho v_S^2}(\mathbf{F} \times \nabla)\left\{\frac{1}{r}\delta\left(t - \frac{r}{v_S}\right)\right\}, \tag{17}$$

respectively. Derivations of the above equations are given in Appendix A of the supporting information. Using (16) and (17), the bracketed terms on the right-hand side of eq. (13) become

$$\nabla \times \nabla \times \{(\nabla \cdot \mathbf{u}(\mathbf{x}))\mathbf{J}\} = \frac{1}{4\pi\rho v_P^2}\left[(\mathbf{J} \cdot \nabla)(\mathbf{F} \cdot \nabla)\nabla\left\{\frac{1}{r}\delta\left(t - \frac{r}{v_P}\right)\right\} - (\mathbf{F} \cdot \nabla)\nabla^2\left\{\frac{1}{r}\delta\left(t - \frac{r}{v_P}\right)\right\}\mathbf{J}\right], \tag{18}$$

$$\nabla \times \nabla \times \{(\mathbf{J} \cdot \nabla)\mathbf{u}(\mathbf{x})\} = \frac{1}{4\pi\rho v_S^2}\left[(\mathbf{J} \cdot \nabla)(\mathbf{F} \cdot \nabla)\nabla\left\{\frac{1}{r}\delta\left(t - \frac{r}{v_S}\right)\right\} - (\mathbf{J} \cdot \nabla)\nabla^2\left\{\frac{1}{r}\delta\left(t - \frac{r}{v_S}\right)\right\}\mathbf{F}\right]. \tag{19}$$

Substituting the above into eq. (10), the governing equation of **B** can be written as

$$\nabla^2 \mathbf{B}(\mathbf{x}, t) - \mu_0\sigma\frac{\partial}{\partial t}\mathbf{B}(\mathbf{x}, t) = +\frac{1}{4\pi}\beta\mu_0\frac{v_S^2}{v_P^2}\left[(\mathbf{J} \cdot \nabla)(\mathbf{F} \cdot \nabla)\nabla\left\{\frac{1}{r}\delta\left(t - \frac{r}{v_P}\right)\right\} - (\mathbf{F} \cdot \nabla)\nabla^2\left\{\frac{1}{r}\delta\left(t - \frac{r}{v_P}\right)\right\}\mathbf{J}\right]$$
$$- \frac{1}{4\pi}\beta\mu_0\frac{3}{2}\left[(\mathbf{J} \cdot \nabla)(\mathbf{F} \cdot \nabla)\nabla\left\{\frac{1}{r}\delta\left(t - \frac{r}{v_S}\right)\right\} - (\mathbf{J} \cdot \nabla)\nabla^2\left\{\frac{1}{r}\delta\left(t - \frac{r}{v_S}\right)\right\}\mathbf{F}\right]. \tag{20}$$

To find the solution, consider a two-variable function a with a parameter v, which satisfies the equation

$$\nabla^2 a(r, t; v) - \mu_0\sigma\frac{\partial}{\partial t}a(r, t; v) = -\frac{1}{r}\delta\left(t - \frac{r}{v}\right), \tag{21}$$

and the condition that $a(r, t; v) = 0$ for $t < 0$. Using the function a, let us consider two vector functions $\mathbf{B}^P$ and $\mathbf{B}^S$, given by

$$\mathbf{B}^P(\mathbf{x}, t) = -\frac{1}{4\pi}\beta\mu_0\frac{v_S^2}{v_P^2}\left[(\mathbf{F} \cdot \nabla)(\mathbf{J} \cdot \nabla)\nabla a(r, t; v_P) - (\mathbf{F} \cdot \nabla)\nabla^2 a(r, t; v_P)\mathbf{J}\right],$$

$$\mathbf{B}^S(\mathbf{x}, t) = \frac{1}{4\pi}\beta\mu_0\frac{3}{2}\left[(\mathbf{F} \cdot \nabla)(\mathbf{J} \cdot \nabla)\nabla a(r, t; v_S) - (\mathbf{J} \cdot \nabla)\nabla^2 a(r, t; v_S)\mathbf{F}\right].$$

By applying the differential operator $\nabla^2 - \mu_0\sigma\,\partial/\partial t$ to both sides, we obtain the differential equations

$$\nabla^2\mathbf{B}^P(\mathbf{x}, t) - \mu_0\sigma\frac{\partial}{\partial t}\mathbf{B}^P(\mathbf{x}, t) = \frac{1}{4\pi}\beta\mu_0\frac{v_S^2}{v_P^2}\left[(\mathbf{F} \cdot \nabla)(\mathbf{J} \cdot \nabla)\nabla\left\{\frac{1}{r}\delta\left(t - \frac{r}{v_P}\right)\right\} - (\mathbf{F} \cdot \nabla)\nabla^2\left\{\frac{1}{r}\delta\left(t - \frac{r}{v_P}\right)\right\}\mathbf{J}\right],$$

$$\nabla^2\mathbf{B}^S(\mathbf{x}, t) - \mu_0\sigma\frac{\partial}{\partial t}\mathbf{B}^S(\mathbf{x}, t) = \frac{1}{4\pi}\beta\mu_0\frac{3}{2}\left[(\mathbf{F} \cdot \nabla)(\mathbf{J} \cdot \nabla)\nabla\left\{\frac{1}{r}\delta\left(t - \frac{r}{v_S}\right)\right\} - (\mathbf{J} \cdot \nabla)\nabla^2\left\{\frac{1}{r}\delta\left(t - \frac{r}{v_S}\right)\right\}\mathbf{F}\right].$$

The sum of the right-hand sides of these two equations is equal to the right-hand side of eq. (20); therefore, the solution to eq. (20) is given by $\mathbf{B}^P + \mathbf{B}^S$:

$$\mathbf{B}(\mathbf{x}, t) = \frac{1}{4\pi}\beta\mu_0\left(-\frac{v_S^2}{v_P^2}\right)\left[(\mathbf{J}\cdot\nabla)(\mathbf{F}\cdot\nabla)\nabla a(r, t; v_P) - (\mathbf{F}\cdot\nabla)\nabla^2 a(r, t; v_P)\mathbf{J}\right]$$

$$+ \frac{1}{4\pi}\beta\mu_0\frac{3}{2}\left[(\mathbf{J}\cdot\nabla)(\mathbf{F}\cdot\nabla)\nabla a(r, t; v_S) - (\mathbf{J}\cdot\nabla)\nabla^2 a(r, t; v_S)\mathbf{F}\right]. \tag{22}$$

It remains to solve eq. (21). To simplify the problem, we can introduce two variables t^* and r^*, defined by

$$r^* \equiv \mu_0\sigma vr,$$
$$t^* \equiv \mu_0\sigma v^2 t, \tag{23}$$

and a two-variable function a^* defined by

$$a^*(r^*, t^*) \equiv \frac{1}{v}a(r, t; v). \tag{24}$$

Eq. (16) is then recast in a form that does not involve v:

$$\nabla^{*2}a^*(r^*, t^*) - \frac{\partial}{\partial t^*}a^*(r^*, t^*) = -\frac{1}{r^*}\delta(t^* - r^*). \tag{25}$$

The analytical solution of this differential equation is given by

$$a^*(r^*, t^*) = \begin{cases} 0 & t^* \leq 0 \\ \frac{1}{2r^*}[q^*(r^*, t^*) - 2 + 2\exp(t^* - r^*)] & 0 < t^* \leq r^* \\ \frac{1}{2r^*}q^*(r^*, t^*) & r^* < t^* \end{cases}, \tag{26}$$

where the function q^* is defined by

$$q^*(r^*, t^*) = \exp(t^* + r^*)\mathrm{erfc}\left(\sqrt{t^*} + \frac{\sqrt{r^*}}{2\sqrt{t^*}}\right) - \exp(t^* - r^*)\mathrm{erfc}\left(\sqrt{t^*} - \frac{\sqrt{r^*}}{2\sqrt{t^*}}\right)$$

$$+ 2\mathrm{erf}\left(\frac{r^*}{2\sqrt{t^*}}\right) + \frac{r^*}{\sqrt{\pi t^{*3}}}\exp\left(-\frac{r^{*2}}{4t^*}\right), \tag{27}$$

and erf and erfc are the error function and complementary error function, respectively (e.g. chapter 13 of Arfken *et al.* 2013), defined by

$$\mathrm{erf}(z) = \frac{1}{\sqrt{\pi}}\int_0^z \exp\left(-z'^2\right)\,dz',$$

$$\mathrm{erfc}(z) = 1 - \mathrm{erf}\,z,$$

respectively. Derivation of this solution is given in Appendix B of the Supporting Information.

Next, an expression is derived for $\mathbf{B}$ for a mechanical source applied at the point $\mathbf{x} = (0, 0, 0)$. Eq. (22) is rewritten in the form

$$B_i(\mathbf{x}, t) = g_{ijk}(\mathbf{r}, t)J_j f_k, \tag{28}$$

where g_{ijk} is a Green's function. The explicit form of g_{ijk} is

$$g_{ijk}(\mathbf{x}, t) = -\frac{1}{4\pi}\mu_0\beta\left[\frac{v_S^2}{v_P^2}\{\partial_i\partial_j\partial_k a(r, t; v_P) - \delta_{ij}\partial_k\nabla^2 a(r, t; v_P)\} - \frac{3}{2}\{\partial_i\partial_j\partial_k a(r, t; v_S) - \delta_{ik}\partial_j\nabla^2 a(r, t; v_S)\}\right]. \tag{29}$$

When a moment tensor $\mathbf{M}$ is the source of the displacement field $\mathbf{u}$, rather than a single force $\mathbf{F}$, $\mathbf{u}$ can be determined by differentiating eq. (14) with respect to x_q and replacing f_p by M_{pq}. The generated magnetic field $\mathbf{B}$ can then be expressed as

$$B_i(\mathbf{x}, t) = g_{ijk,l}(\mathbf{x}, t)J_j M_{kl}, \tag{30}$$

where $g_{ijk,l}(\mathbf{x}, t) \equiv \partial g_{ijk}(\mathbf{x}, t)/\partial x_l$.

3.3 Step response of the magnetic field

In general, applied single forces and double-couple sources depend on time, and have a finite spatial extent. The general expression for the generated magnetic field is

$$B_i(\mathbf{x}, t) = \int_{-\infty}^t dt' \int_{V'} dV(\mathbf{x}')g_{ijk,l}(\mathbf{x} - \mathbf{x}', t - t')J_j M_{kl}(\mathbf{x}', t'), \tag{31}$$

where V' is the source volume. When temporal variations in M_{kl} can be expressed using the Heaviside step function H by

$$M_{kl}(\mathbf{x}', t') = \sum_{n=1}^{N} M_{kl}^{(n)} \delta^3(\mathbf{x}' - \mathbf{x}'^{(n)}) H(t' - t'^{(n)}),$$

(32)

the expression for B_i becomes

$$B_i(\mathbf{x}, t) = \sum_{n=1}^{N} G_{ijk,l}(\mathbf{x} - \mathbf{x}', t - t') J_j M_{kl},$$

(33)

where $G_{ijk,l}$ are defined by

$$G_{ijk,l}(\mathbf{x}, t) = -\frac{1}{4\pi} \mu_0 \beta \left[\frac{v_S^2}{v_P^2} \{ \partial_i \partial_j \partial_k \partial_l A(r, t; v_P) - \delta_{ij} \partial_k \partial_l \nabla^2 A(r, t; v_P) \} - \frac{3}{2} \{ \partial_i \partial_j \partial_k \partial_l A(r, t; v_S) - \delta_{ik} \partial_j \partial_l \nabla^2 A(r, t; v_S) \} \right],$$

(34)

and

$$A(r, t; v) \equiv \int_{-\infty}^{t} a(r, t'; v) H(t') \mathrm{d}t' = \int_{0}^{t} a(r, t'; v) \mathrm{d}t'.$$

(35)

Using the regularized parameters r^* and t^* from eq. (23), the explicit form of A is given by

$$A(r, t; v) = \frac{1}{\mu_0 \sigma v} A^*(r^*, t^*)$$

(36)

with the function A^* defined by

$$A^*(r^*, t^*) = \frac{1}{2r^*} \times \begin{cases} Q^*(r^*, t^*) - 2t^* + 2\exp(t^* - r^*) - 2\exp(-r^*) & t^* \le r^* \\ Q^*(r^*, t^*) - 2r^* + 2 - 2\exp(-r^*), & t^* > r^* \end{cases}$$

(37)

and Q^* defined by

$$\begin{aligned} Q^*(r^*, t^*) &\equiv \int_{0}^{t^*} q^*(r^*, t^*) \mathrm{d}t'^* \\ &= \exp(t^* + r^*) \mathrm{erfc}\left(\sqrt{t^*} + \frac{r^*}{2\sqrt{t^*}}\right) - \exp(t^* - r^*) \mathrm{erfc}\left(\sqrt{t^*} - \frac{r^*}{2\sqrt{t^*}}\right) \\ &\quad - 2\,\mathrm{erfc}\left(\frac{r^*}{2\sqrt{t^*}}\right) - r^{*2} \mathrm{erfc}\left(\frac{r^*}{2\sqrt{t^*}}\right) + 2r^* \frac{\sqrt{t^*}}{\sqrt{\pi}} \exp\left(-\frac{r^{*2}}{4t^*}\right) \\ &\quad + 2\exp(-r^*) + 2t^* \mathrm{erf}\left(\frac{r^*}{2\sqrt{t^*}}\right). \end{aligned}$$

(38)

In certain extreme situations, the spatial derivative of A^* has an especially simple form. Let us analytically consider some of these special cases. The final expression of **B** contains only the spatial derivatives of A; thus, it is only necessary to evaluate $\partial A / \partial r$. By considering the asymptotic behaviour of A^* at $t^* \gg 1$, we have

$$\lim_{t^* \to \infty} \frac{\partial}{\partial r^*} A^*(r^*, t^*) = -\frac{1}{2}.$$

(39)

We can also evaluate A in cases where σ is very small; here, r^* and t^* are also small because of their definition (eq. 23). By considering the Taylor's series expansion of A^* for small values of r^* and t^*, we obtain the expression

$$\lim_{\sigma \to +0} \frac{\partial}{\partial r^*} A^*(r^*, t^*) = \begin{cases} -\frac{t^{*2}}{2r^{*2}} & t^* \le r^*, \\ -\frac{1}{2} & t^* > r^*. \end{cases}$$

(40)

Note that $\partial A^* / \partial r^* = \partial A / \partial r$ because of the definitions of A^* and r^*. As $t \to \infty$ and $\sigma \to 0$, $\partial A^* / \partial r^*$ converges to the same value and does not depend on σ or v. This is as expected, because these values should be equal to that of the static problem, which should not depend on the electrical conductivity or elastic properties of the medium.

4 NUMERICAL EXAMPLES

Using the formulas derived above, some numerical examples are now considered to explore the behaviour of the solutions. Two example geometries (i.e. combinations of directions of double-couple moment tensor and initial magnetization) are shown in Figs 1(a) and (b). The direction from the epicentre to the site (i.e. X-axis) lies in the plane in which mechanical forces act in the first geometry (i.e. the X–Y plane), and perpendicular to this plane in the second geometry (i.e. the Y–Z plane). Because of the symmetry of the solution, only the x-component of $\Delta \mathbf{B}$ (B_x) for geometry 1 and the y-component of $\Delta \mathbf{B}$ (B_y) for geometry 2 have non-zero values.

In the calculation, the following parameter values are employed. The values of stress sensitivity and P-wave velocity for these examples are $\beta = 2 \times 10^{-9}$ Pa^{-1} and $v_P = 5 \times 10^3$ m s^{-1}, respectively. The crust is assumed to be a Poisson solid, for which $v_P / v_S = \sqrt{3}$. The seismic
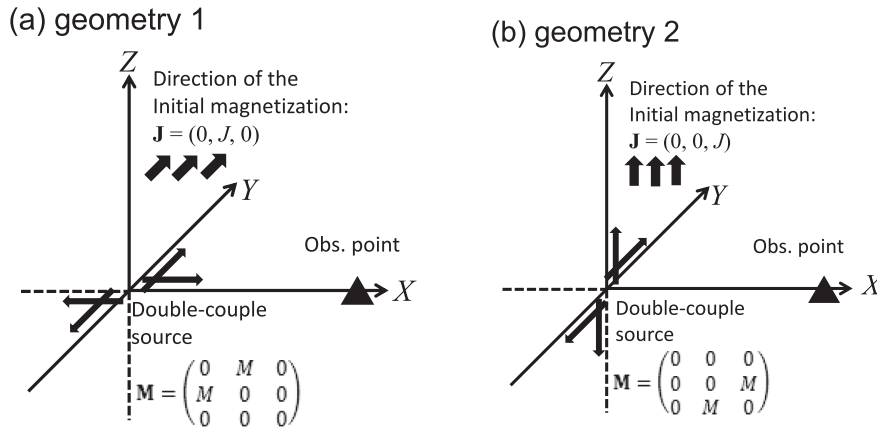
(a) geometry 1

(b) geometry 2

Figure 1. Two geometries considered in numerical examples. Both the observation point and the source are on the *x*-axis in both cases. (a) Geometry 1: The non-zero component of **M** is $M_{12} = M_{21} = M$ and the initial magnetization is $\mathbf{J} = (0, J, 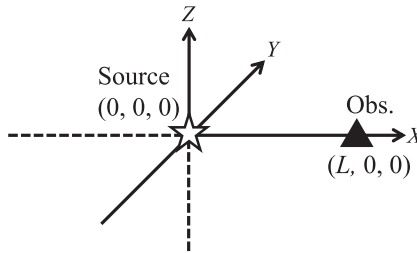0)$. The generated magnetic field only has an *x*-component. (b) Geometry 2: The non-zero component of is $M_{23} = M_{32} = M$ and the initial magnetization is $\mathbf{J} = (0, 0, J)$. The generated magnetic field only has a *y*-component.

Figure 2. Source and receiver for a source approximated by a single point.

moment (M) is set to 4.0×10^{19} Nm, which corresponds to M_w 7 earthquakes. Results are determined for four values of electrical conductivity ($\sigma = 1 \times 10^{-1}$, 10^{-2}, 10^{-3} and 10^{-4} S m^{-1}, respectively), which correspond to the possible range of values in the Earth's crust. Note that the expression for $\Delta\mathbf{B}$ (eq. 22) does not depend on rigidity, as long as we fix the seismic moment.

As the simplest model, consider a source approximated by a single point (Fig. 2). Two source–time functions are considered: a step function (Fig. 3a) and a ramp function (Fig. 3b). The source distance $L = 25$ km, meaning that the *P*-wave arrives at $t = 5.0$ s. Numerical examples corresponding to the step and ramp source–time functions are given in Figs 4 and 5, respectively. Results for the ramp source–time function were obtained by summing the results of step functions.

As a more realistic model, cases are considered in which the source consists of multiple points (Fig. 6). Fig. 7 shows two illustrative examples in which a rupture propagates toward (Fig. 7a) and away (Fig. 7b) from the observation site. The source distance L, measured from the centre of the sources to the observation point, is set to 25 km, meaning that the *P* wave arrives at $t = 6.0$ s in the first example (Fig. 7a), and $t = 4.0$ s in the second (Fig. 7b). Numerical examples corresponding to the first and second situations are shown in Figs 8 and 9, respectively.

Note that the magnetic field arising from any double-coupled moment and initial magnetization, with the same intensity but an arbitrary direction, can be found by rotating the results. Thus, the above examples are sufficient to describe the piezomagnetic effect for an arbitrarily rotated geometry.
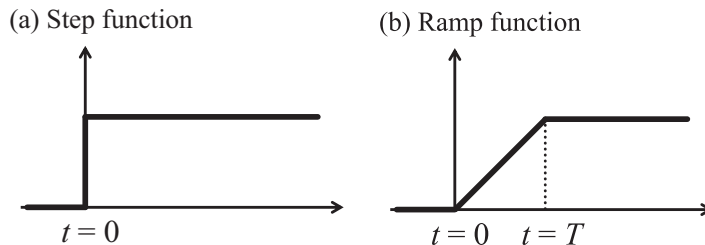
(a) Step function   (b) Ramp function

Figure 3. Schematics explaining the point source problem considered in the numerical example. (a) A source–time function given by a step function. (b) A source–time function given by a ramp function. In these examples, *L* and *T* are set to 25 km and 10 s, respectively.

(a) B_x for geometry 1
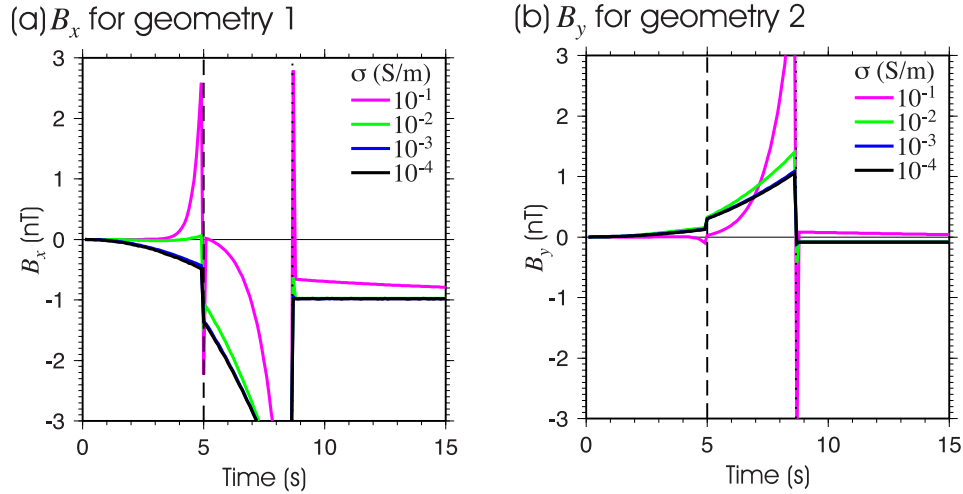

(b) B_y for geometry 2

Figure 4. Temporal variations in the generated magnetic field when the source–time function is a ramp function. In the calculations, the ramp function is approximated by multiple step functions with intervals of 0.05 s. In this figure, and in Figs 5, 8, and 9, subpanels (a) and (b) show results for geometries 1 and 2 (see Fig. 1), respectively, and broken and dashed lines represent S- and P-wave arrival times, respectively.
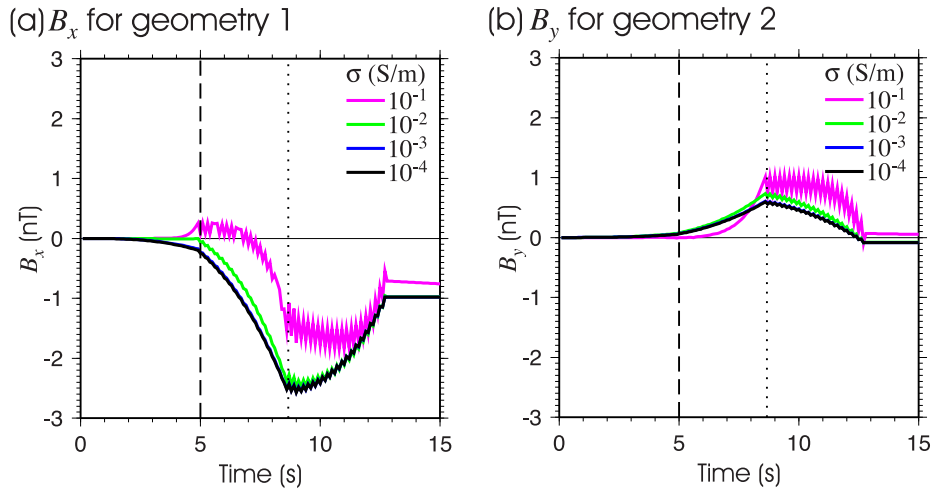
(a) B_x for geometry 1

(b) B_y for geometry 2

Figure 5. Temporal variations in the generated magnetic field when the source–time function is a ramp function. The jagged shapes in the curves are artefacts due to the step approximation of the ramp function.

5 DISCUSSION

The following discussion considers the characteristics of magnetic 'early signals' generated by the piezomagnetic field ($\Delta\mathbf{B}$). Here, 'early signals' mean temporal variations in $\Delta\mathbf{B}$ before the arrival of the seismic P wave. In addition, after a P-wave arrival, observation of $\Delta\mathbf{B}$ is generally difficult because the seismic waves induce mechanical vibrations in magnetic sensors. Therefore, it is of interest to focus on 'early signals'; that is, $\Delta\mathbf{B}$ before the P-wave onset.

Let us examine the dependency of $\Delta\mathbf{B}$ on electrical conductivity (σ). The numerical examples in Figs 4, 5, 8 and 9 demonstrate that temporal variations in $\Delta\mathbf{B}$ are quite different for different values of σ. In a highly conductive medium (i.e. $\sigma = 10^{-1}$ S m^{-1}), signals only appear just before the P-wave arrival. In resistive media (i.e. $\sigma = 10^{-4}$ or 10^{-3} S m^{-1}), the rise time of EM signals is earlier than for a
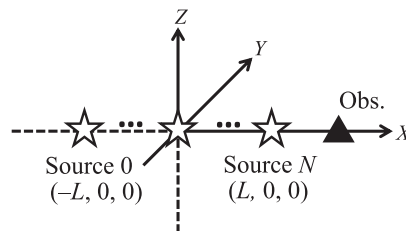

Figure 6. Locations of sources and receivers considered in the multiple source problem.
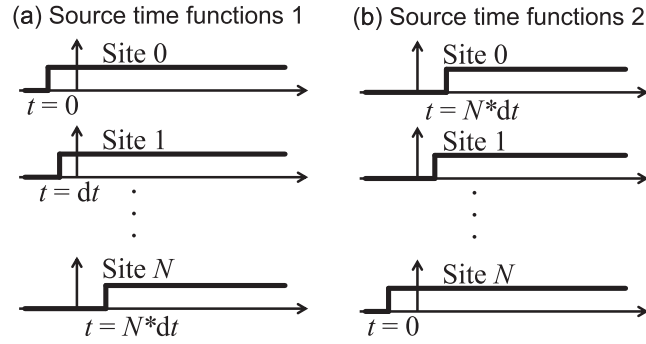
Figure 7. Two sets of source time functions considered in the multiple source problem. Sites 0 to N correspond to sites in Fig. 6. The set shown in (a) represents the case where rupture propagates toward the site. In (b), rupture propagates away from the site.
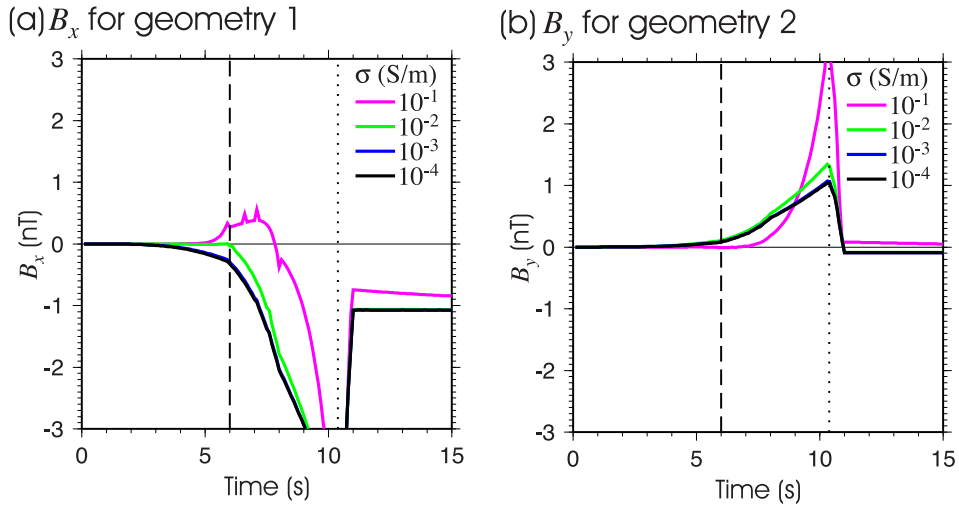

Figure 8. Temporal variations in the generated magnetic field when the source location moves in the $+x$ direction (i.e. toward the receiver).

conductive medium. In some cases, even the polarities (i.e. signs of B_x or B_y) of early signals are different for conductive and resistive models (e.g. Figs 4, 5a, 8a and 9a).

   The differences between rise times in conductive and resistive media can be interpreted as follows. Using the diffusion equation for $\Delta \mathbf{B}$ (eq. 10), we can estimate that large changes in $\Delta \mathbf{B}$ will appear approximately $T = \mu_0 \sigma X^2$ seconds after the source (i.e. right-hand side of eq. 10) appears. At $X = 25 \times 10^3$ m, $T = 0.05, 0.5, 5$ and 50 s for $\sigma = 10^{-4}, 10^{-3}, 10^{-2}$ and 10^{-1} S m^{-1}, respectively. A large $\Delta \mathbf{B}$ appears well before the P-wave arrival time (T_P) for $\sigma = 10^{-4}$ and 10^{-3} S m^{-1}, and well after T_P for $\sigma = 10^{-1}$ S m^{-1}.
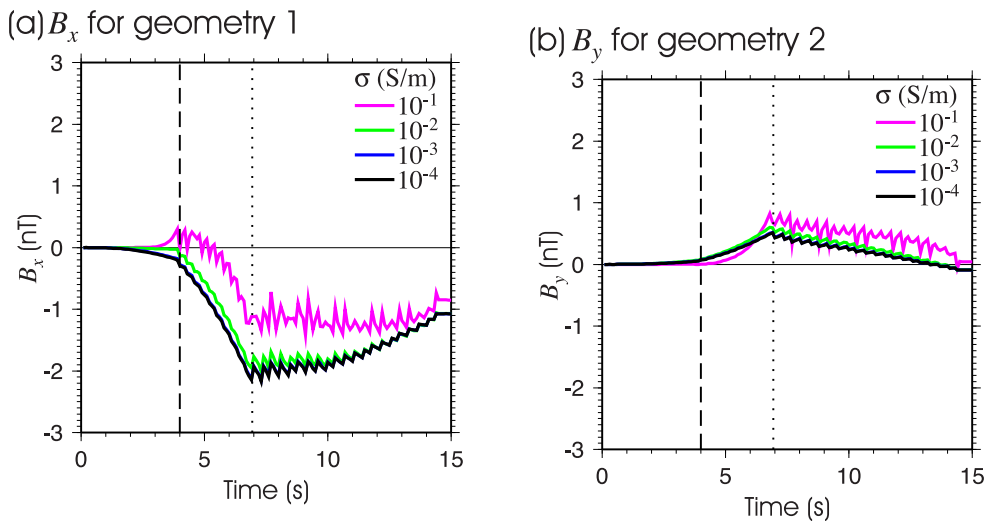

Figure 9. Temporal variations in the generated magnetic field when the source location moves in the $-x$ direction (i.e. away from the receiver).

The high dependency on electrical conductivity means that precise calculation of $\Delta\mathbf{B}$ is difficult unless the conductivity of the crust is uniform. If we ignore the electrical conductivity, estimates of $\Delta\mathbf{B}$ will be considerably different from actual values. Moreover, the electrical conductivity of the Earth's crust is generally heterogeneous, which makes precise estimation a difficult problem. It is natural to expect that assuming a heterogeneous structure would considerably alter estimates of $\Delta\mathbf{B}$. Therefore, accurate estimation of $\Delta\mathbf{B}$ is difficult in general. Nevertheless, it is meaningful to estimate the amplitudes of early $\Delta\mathbf{B}$ signals, as this will help us to understand whether observed early signals in the magnetic field (e.g. Okubo *et al.* 2011) could arise from the piezomagnetic effect.

If the source is a point (e.g. Fig. 2) and the source–time function is a step function (Fig. 3a), then the expected amplitude of $\Delta\mathbf{B}$ is large enough to observe. We can refer to Fig. 4 to observe the expected result. When the medium is resistive ($\sigma = 10^{-4}$ or 10^{-3} S m^{-1}), the early signal of $\Delta\mathbf{B}$ is emergent, but reaches 0.5 nT before the seismic wave arrival (i.e. $t = 5$ s). The amplitude of 0.5 nT is approximately half of the piezomagnetic field at $t = \infty$. When the medium is conductive ($\sigma = 10^{-4}$ S m^{-1}), the large early signal ($\geq$0.5 nT) appears only in the last 0.1 s before the *P*-wave arrival, but reaches amplitudes as large as 2.5 nT. In both cases, the amplitude is large enough to be observed.

However, from Figs 5, 8 and 9, the amplitudes of $\Delta\mathbf{B}$ for the step source–time function are probably overestimated. If the source is a point (Fig. 2) and the source time function is a ramp function (Fig. 3b), then expected early signals of $\Delta\mathbf{B}$ are hardly large enough to observe. We can refer to Fig. 5 to observe the result: in both conductive and resistive media, the early signal is emergent and the amplitude is as small as 0.3 nT, smaller than for a step function. Because complete fault rupture is not instantaneous but occurs over a finite duration of time, the ramp function is more appropriate than the step function for representing real seismic source processes. Therefore, it is likely that Fig. 5 captures the piezomagnetic effect more realistically than Fig. 4.

Even when the spatial extent of the sources is considered, the expected amplitudes of $\Delta\mathbf{B}$ are not considerably enhanced. When a source consists of multiple points (Fig. 6) and the moment release occurs successively (Fig. 7), early signals are as large as 0.3 nT. The amplitudes are similar to those obtained for a ramp function (Fig. 5), although the waveforms are different. This example is rather simple; however, it demonstrates that no prominent rupture directivity effect, like that which appears in seismology (e.g. fig. 3.1 of Agarwal & Shrikhande 2006), is expected for early EM signals.

Based on these discussions, it is concluded that observation of the early signal is generally difficult. The numerical calculation is performed by assuming a moment magnitude of 7. With increasing moment magnitude, the total amount of expected EM signals should increase. However, the situation is different when we focus on early EM signals. Note that only the moment released in the few seconds after the onset of rupture contributes to the generation of early EM signals. Even for a M_w 9 earthquake, the seismic moment released during the first 10 s is not very large (e.g. Ammon *et al.* 2005; Koketsu *et al.* 2011), being comparable to a M_w 7 earthquake. Therefore, the early EM signals of M_w 8 or M_w 9 earthquakes are unlikely to be much larger than those for M_w 7 earthquakes.

Because of uncertainty about the piezomagnetic stress sensitivity (β), that the above examples, which reflect rather poorly on signal detectability, may be incorrect. I used $\beta = 2.0 \times 10^{-9}$ Pa^{-1} in the numerical examples, a typical value for studies of the piezomagnetic effect (e.g. Sasai 1991). However, simulations using this value underestimate the observed piezomagnetic field in many cases (e.g. Zhan 1989; Oshiman *et al.* 1990; Nishida *et al.* 2004). Moreover, it has been proposed that β depends on the timescale of stress change (Uyeshima 2007). Because amplitudes of $\Delta\mathbf{B}$ are proportional to β, we cannot draw definite conclusions about the amplitude of $\Delta\mathbf{B}$ until values of β in the real Earth are more precisely determined.

The effects of heterogeneities on initial magnetization should also be noted. Heterogeneous initial magnetization enhances the signal strength of the piezomagnetic effect (e.g. Oshiman 1990; Yamazaki 2011b). Therefore, observations at suitable locations may detect magnetic signals arising from the piezomagnetic effect, which could enable the detection of seismic events before the first seismic waves arrive. Quantitative discussion of this possibility is beyond the scope of this study, but will be the subject of future work.

6 CONCLUSIONS

A set of analytical expressions was derived for EM signals generated by the piezomagnetic effect for a double-couple seismic source. Numerical examples calculated using the obtained formula resolve quantitative features of the expected magnetic field. Temporal variations in the magnetic field depend strongly on the electrical conductivity of the medium, meaning that precise determinations of piezomagnetic effect amplitudes are generally difficult. The expected amplitudes of piezomagnetic signals that precede the arrival of seismic waves are no larger than 0.3 nT for earthquakes with a moment magnitude of $\geq$7.0 at a source distance of 25 km. However, this may underestimate the expected amplitude of signals, because the true value of piezomagnetic stress sensitivity remains poorly constrained.

REFERENCES

Abdul Azeez, K.K., Manoj, C., Veeraswamy, K. & Harinarayana, T., 2009. Co-seismic EM signals in magnetotelluric measurement—a case study during Bhuj earthquake (26th January 2001), India, *Earth Planets Space,* **61,** 973–981.

Agarwal, P. & Shrikhande, M., 2006. *Earthquake Resistant Design of Structures,* PHI Learning Pvt. Ltd., 660 pp.

Aki, K. & Richards, P.G., 2002. *Quantitative Seismology,* 2nd edn, University Science Books, 704 pp.

Ammon, C.J. *et al.*, 2005. Rupture process of the 2004 Sumatra–Andaman earthquake, *Science,* **308,** 1133–1139.

Arfken, G.B., Weber, H.J. & Harris, F.E., 2013. *Mathematical Methods for Physics: A Comprehensive Guide,* 7th edn, Academic Press, 1220 pp.

Bishop, J.R., 1981. Piezoelectric effects in quartz-rich rocks, *Tectonophysics.*, **77,** 297–321.

Eleman, F., 1965. The response of magnetic instruments to earthquake waves, *J. Geomag. Geoelectr.,* **18,** 43–72.

Gao, Y., Chen, X., Hu, H. & Zhang, J., 2013a. Early electromagnetic waves from earthquake rupturing: I. Theoretical formulations, *Geophys. J. Int.,* **192,** 1288–1307.

Gao, Y., Chen, X., Hu, H. & Zhang, J., 2013b. Early electromagnetic waves from earthquake rupturing: II. Validation and numerical experiments, *Geophys. J. Int.,* **192,** 1308–1323.

Gao, Y., Chen, X., Hu, H., Wen, J., Tang, J. & Fang, G., 2014. Induced electromagnetic field by seismic waves in Earth's magnetic field, *J. geophys. Res.,* **119,** 5651–5685.

Garambois, S. & Dietrich, M., 2001. Seismoelectric wave conversions in porous media: field measurements and transfer function analysis, *Geophys.*, **66,** 1417–1430.

Garambois, S. & Dietrich, M., 2002. Full waveform numerical simulations of seismoelectromagnetic wave conversions in fluid-saturated stratified porous media, *J. geophys. Res.: Solid Earth,* **107,** doi:10.1029/2001JB000316.

Gershenzon, N.I. & Bambakidis, G., 2001. Modeling of seismo-electromagnetic phenomena, *Russ. J. Earth Sci.,* **3,** 247–275.

Gershenzon, N.I., Gokhberg, M.B. & Yunga, S.L., 1993. On the electromagnetic field of an earthquake focus, *Phys. Earth planet. Inter.,* **77,** 13–19.

Gershenzon, N.I., Bambakidis, G. & Ternovskiy, I., 2014. Coseismic electromagnetic field due to the electrokinetic effect, *Geophysics,* **79,** E217–E229.

Haartsen, M.W. & Pride, S.R., 1997. Electroseismic waves from point sources in layered media, *J. geophys. Res.,* **102,** 24 745–24 769.

Honkura, Y., Ogawa, Y., Matsushima, M., Nagaoka, S., Ujihara, N. & Yamawaki, T., 2009. A model for observed circular polarized electric fields coincident with the passage of large seismic waves, *J. geophys. Res.,* **114,** doi:10.1029/2008JB006117.

Huang, Q., 2002. One possible generation mechanism of co-seismic electric signals, *Proc. Jpn. Acad., Ser. B,* **78,** 173–178.

Ishido, T. & Mizutani, H., 1981. Experimental and theoretical basis of electrokinetic phenomena in rock-water systems and its applications to geophysics, *J. geophys. Res.,* **86,** 1763–1775.

Koketsu, K. *et al.*, 2011. A unified source model for the 2011 Tohoku earthquake, *Earth planet. Sci. Lett.,* **310,** 480–487.

Kuriki, M., Matsushima, M., Ogawa, Y. & Honkura, Y., 2011. Spectral peaks in electric field at resonance frequencies for seismically excited motion of ions in the Earth's magnetic field, *Earth Planets Space,* **63,** 503–507.

Matsushima, M., Honkura, Y., Kuriki, M. & Ogawa, Y., 2013. Circularly polarized electric fields associated with seismic waves generated by blasting, *Geophys. J. Int.,* **194,** 200–211.

Nabighian, M.N., 1988. *Electromagnetic Methods in Applied Geophysics,* SEG Books, 972 pp.

Nagao, T., Orihara, Y., Yamaguchi, T., Takahashi, I., Hattori, K., Noda, Y. & Sayanagi, K., 2000. Co-seismic geoelectric potential changes observed in Japan, *Geophys. Res. Lett.,* **27,** 1535–1538.

Nagata, T., 1970. Basic magnetic properties of rocks under the effects of mechanical stresses, *Tectonophys.*, **9,** 167–195.

Napoli, R., Currenti, G., Del Negro, C., Greco, F. & Scandura, D., 2008. Volcanomagnetic evidence of the magmatic intrusion on 13th May 2008 Etna eruption, *Geophys. Res. Lett.,* **35,** doi:10.1029/2008GL035350.

Nishida, Y., Sugisaki, Y., Takahashi, K., Utsugi, M. & Oshima, H., 2004. Tectonomagnetic study in the eastern part of Hokkaido, NE Japan: discrepancy between observed and calculated results, *Earth Planets Space,* **56,** 1049–1058.

Ogawa, T. & Utada, H., 2000a. Coseismic piezoelectric effects due to a dislocation 1. An analytic far and early-time field solution in a homogeneous whole space, *Phys. Earth planet. Inter.,* **121,** 273–288.

Ogawa, T. & Utada, H., 2000b. Electromagnetic signals related to incidence of a teleseismic body wave into a subsurface piezoelectric body, *Earth Planet Space,* **52,** 253–260.

Okubo, K., Takeuchi, N., Utsugi, M., Yumoto, K. & Sasai, Y., 2011. Direct magnetic signals from earthquake rupturing: Iwate–Miyagi earthquake of M 7.2, Japan. *Earth planet. Sci. Lett.,* **305,** 65–72.

Oshiman, N., 1990. Enhancement of tectonomagnetic change due to non-uniform magnetization in the earth's crust—two-dimensional case studies, *J. Geomag. Geoelectr.,* **42,** 607–619.

Oshiman, N., Sasai, Y., Miyakoshi, J., Nishida, R. & Shiozaki, I., 1990. Continuous observation of piezomagnetic changes due to ground loading by Lake Nichinan, Tottori, Japan, in *Proceedings of the Conductivity Anomaly Symposium (1991)*, Japan, pp. 137–148 (in Japanese).

Ren, H.X., Chen, X.F. & Huang, Q.H., 2012. Numerical simulation of co-seismic electromagnetic fields associated with seismic waves due to finite faulting in porous media, *Geophys. J. Int.,* **188,** 925–944.

Pride, S., 1994. Governing equations for the coupled electromagnetics and acoustics of porous media, *Phys. Rev. B,* **50,** 15 678–15 695.

Pride, S.R. & Haartsen, M.W., 1996. Electroseismic wave properties, *J. acoust. Soc. Am.,* **100,** 1301–1315.

Russell, R.D. & Barker, A.S.J., 1991. Seismo-electric exploration: expected signal amplitudes, *Geophys. Prospect.,* **39,** 105–118.

Sasai, Y., 1991. Tectonomagnetic modeling on the basis of the linear piezomagnetic effect, *Bull. Earthq. Res. Inst., Univ. Tokyo,* **66,** 585–722.

Sasai, Y. & Ishikawa, Y., 1997. Seismomagnetic models for earthquakes in the eastern part of Izu Peninsula, Central Japan, *Ann. Geophys.,* **40,** 463–478.

Skordas, E., Kapiris, P., Bogris, N. & Varotsos, P., 2000. Field experimentation on the detectability of co-seismic electric signals, *Proc. Jpn. Acad., Ser. B,* **76,** 51–56.

Stacey, F.D., 1964. The seismomagnetic effect, *Pure appl. Geophys.,* **58,** 5–22.

Stacey, F.D. & Johnston, M.J.S., 1972. Theory of the piezo-magnetic effect in titanomagnetite-bearing rocks, *Pure appl. Geophys.,* **97,** 146–155.

Stuart, W.D., Banks, P.O., Sasai, Y. & Liu, S.-W., 1995. Piezornagnetic field for Parkfield fault model, *J. geophys. Res.,* **100,** 24 101–24 110.

Ueda, H., Matsumoto, T., Fujita, E., Ukawa, M., Yamamoto, E., Sasai, Y., Irwan, M. & Kimata, F., 2006. Geomagnetic changes associated with the dike intrusion during the 2000 Miyakejima eruptive activity, Japan, *Earth planet. Sci. Lett.,* **245,** 416–426.

Utsugi, M., 2010. Formulation of the piezomagnetic effect considering the seismic wave propagation, in *Paper Presented at Japan Geoscience Union (JpGU) Meeting 2010*, Makuhari, Chiba, Japan, 2010 May 23–28.

Utsugi, M., Nishida, Y. & Sasai, Y., 2000. Piezomagnetic potentials due to an inclined rectangular fault in a semi-infinite medium, *Geophys. J. Int.,* **140,** 479–492.

Uyeshima, M., 2007. EM monitoring of crustal processes including the use of the Network-MT observations, *Surv. Geophys.,* **28,** 199–237.

Wessel, P. & Smith, W.H.F., 1998. New, improved version of Generic Mapping Tools released, *EOS, Trans. Am. geophys. Un.,* **79,** 579.

Yamazaki, K., 2011a. Piezomagnetic fields arising from the propagation of teleseismic waves in magnetized crust with finite conductivity, *Geophys. J. Int.,* **184,** 626–638.

Yamazaki, K., 2011b. Enhancement of co-seismic piezomagnetic signals near the edges of magnetization anomalies in the Earth's crust, *Earth Planet Space,* **63,** 111–118.

Yamazaki, K., 2012. Estimation of temporal variations in the magnetic field arising from the motional induction that accompanies seismic waves at a large distance from the epicenter, *Geophys. J. Int.,* **190,** 1393–1403.

Zhan, Z., 1989. Investigations of tectonomagnetic phenomena in China, *Phys. Earth planet. Inter.,* **57,** 11–22.

Zlotnicki, J., Pozzi, J.P. & Cornet, F.H.C., 1981. Investigation on induced magnetization variations caused by triaxial stresses, *J. geophys. Res.,* **86,** 11 899–11 909.

SUPPORTING INFORMATION

Additional Supporting Information may be found in the online version of this paper:

Appendix A: Proof of eqs (16) and (17)
Appendix B: Solution of eq. (26).
Figure B1. Integral paths on the complex plane.
(http://gji.oxfordjournals.org/lookup/suppl/doi:10.1093/gji/ggw125/-/DC1).

Please note: Oxford University Press is not responsible for the content or functionality of any supporting materials supplied by the authors. Any queries (other than missing material) should be directed to the corresponding author for the paper.